Article

Synthesis, Characterization, and Performance Evaluation of Hybrid Waste Sludge Biochar for COD and Color Removal from Agro-Industrial Effluent

Ahmad Hussaini Jagaba [1,2,*], Shamsul Rahman Mohamed Kutty [1], Sule Abubakar [2], Abdullahi Haruna Birniwa [3], Ibrahim Mohammed Lawal [2,4], Ibrahim Umaru [2], Abdullahi Kilaco Usman [5], Nura Shehu Aliyu Yaro [1,6], Nabil Al-Zaqri [7], Basheer M. Al-Maswari [8], Mohamad Nasir Mohamad Ibrahim [9] and Fida Hussain [10,*]

[1]   Department of Civil and Environmental Engineering, Universiti Teknologi PETRONAS, Bandar Seri Iskandar 32610, Malaysia
[2]   Department of Civil Engineering, Abubakar Tafawa Balewa University, Bauchi 740272, Nigeria
[3]   Department of Chemistry, Sule Lamido University, Kafin-Hausa 741103, Nigeria
[4]   Department of Civil and Environmental Engineering, University of Strathclyde, Glasgow G1 1XJ, UK
[5]   School of Civil Engineering, Universiti Teknologi Malaysia, Johor Bahru 81310, Malaysia
[6]   Department of Civil Engineering, Ahmadu Bello University, Zaria 810107, Nigeria
[7]   Department of Chemistry, College of Science, King Saud University, Riyadh 11451, Saudi Arabia
[8]   Department of Chemistry, Yuvaraja's College, University of Mysore, Mysuru 570005, India
[9]   Materials Technology Research Group (MaTRec), School of Chemical Sciences, Universiti Sains Malaysia (Minden), George Town 11800, Malaysia
[10] Research Institute for Advanced Industrial Technology, College of Science and Technology, Korea University, Sejong 30019, Korea
*   Correspondence: ahjagaba@gmail.com (A.H.J.); hussainfida@korea.ac.kr (F.H)

Abstract: Agro-waste management processes are evolving through the development of novel experimental approaches to understand the mechanisms in reducing their pollution levels efficiently and economically from industrial effluents. Agro-industrial effluent (AIE) from biorefineries that contain high concentrations of COD and color are discharged into the ecosystem. Thus, the AIE from these biorefineries requires treatment prior to discharge. Therefore, the effectiveness of a continuous flow bioreactor system (CFBS) in the treatment of AIE using hybrid waste sludge biochar (HWSB) was investigated. The use of a bioreactor with hydraulic retention time (HRT) of 1–3 days and AIE concentrations of 10–50% was used in experiments based on a statistical design. AIE concentration and HRT were optimized using response surface methodology (RSM) as the process variables. The performance of CFBS was analyzed in terms of COD and color removal. Findings indicated 76.52% and 66.97% reduction in COD and color, respectively. During biokinetic studies, the modified Stover models were found to be perfectly suited for the observed measurements with R^2 values 0.9741 attained for COD. Maximum contaminants elimination was attained at 30% AIE and 2-day HRT. Thus, this study proves that the HWSB made from biomass waste can potentially help preserve nonrenewable resources and promote zero-waste attainment and principles of circular economy.

Keywords: agro-industrial effluent; biochar; chemical oxygen demand; color; palm-oil mill-effluent sludge; pulp and paper sludge

1. Introduction

Agro-industries have increased more than thrice over the past five decades as a consequence of improved agricultural soil, technical advancements brought about by the green revolution, and growing population that was expedited [1]. Agro-industries are one of the largest contributors to the global economy, producing an estimated mean value of 23.7 million tonnes of food every day, particularly in developing countries that frequently

rely on subsistence farming and income from formal and/or unofficial agro-industries. The industries produce much biomass, which is a key component of the bioeconomy. They are also a significant contributor to the issue of environmental contamination on a global scale [2]. Considering the rapid rate of population development, excess utilization of natural resources, and rising energy consumption per individual, it is frequently unavoidable that highly sophisticated, renewable, and affordable wastes from agro-industries will increase. Their primary structural elements contain significant amounts of lignin, hemicelluloses, starch, and cellulose [3]. Modern trends have seen a drive toward waste transformation into useful resources rather than simply treatment to create a more sustainable society. Thus, it leads to the generation of agro-industrial effluents (AIE) at high rates and volumes.

Sugarcane, grains, oilseeds, cassava, milk, and animal slaughter are the primary sources of products from the agro-industrial sectors. Large quantities of energy, water, and soil are needed for these processes [4]. Consequently, considerable amounts of solid waste and effluents with major pollution-causing qualities are produced. The produced AIE include fruit, cassava, potato, vinasse, coffee, dairy, cheese whey, beverage, palm oil, winery, elderberry juice production effluent, slaughterhouse effluents, and olive mill and pulp and paper mill wastewaters. The raw materials' source, products' nature, operations, and the phases in the processing all affect the composition and quantity of AIE [5]. Although their physicochemical characteristics are quite diverse, even among those of the same origin, they generally consist of organic and inorganic pollutants present in high concentrations, nutrients (nitrogen, phosphorus, and potassium), toxic compounds (including heavy metals), pesticides, phenols, and components that may influence air, water, and soil quality. They include a significant number of organic compounds with high COD and color values, which have the potential to result in serious pollution issues [6]. The treatment of these effluents presents an environmental challenge because of the high pollutant load, vast volumes produced, and seasonal fluctuation. Thus, when released without receiving proper treatment, the effluent poses a serious threat to the environment [7]. Therefore, SDG 12's target 12.5 for this goal highlights waste management as a worldwide concern.

The unregulated discharge of untre"ted 'IE Into the environment can promote eutrophication processes, ecosystem imbalance, and pose detrimental effects to humans, animals, and plants. There is possible risk that it will contaminate shallow and groundwater aquifers and cause serious environmental issues due to its accumulation in soil and water habitats [2], thus rendering the absorbing bodies of water unsuitable for other applications. Diverse ecological systems may be greatly affected by these effluents, which can lead to changes in soil physical/chemical properties and soil microbial population, unpleasant odors, water resource depletion, dissemination of endemic diseases, and dissolved oxygen depletion in water. It increases salt content in soil, increases the temperature of receiving water bodies, and can cause soil contamination by toxic ions/compounds and metals [8]. The production and release of various greenhouse gases is an additional concerning effect of effluents (CH_4 and CO_2). Twenty-one percent of all greenhouse gas emissions are attributable to it. Acid rain is also caused by the re-release of NO_x and SO_x [9]. AIEs must first undergo chemical and biological treatment due to their significant eutrophic and polluting potential before disposal into the environment. AIE should therefore be carefully treated with the intention of recovering, valuing, or removing the pollutant load before disposal.

AIE reclamation not only provides a remarkable volume of irrigation water, but also contributes to mitigate/decrease water shortage, conserve potable resources, support the agriculture sector, protects groundwater resources, and reduces the environmental impact related to the effluent discharge into water bodies [10]. In light of the risk of climate change and other environmental problems, AIE management strategies are changing. AIE treatment is receiving much attention currently because of its potential to mitigate pollution resulting from rapid industrialization and other anthropogenic activities. There are numerous AIE treatment options available. However, to adhere to the legal restrictions of release in sewer systems and/or in natural waters, continuously looking for cost-effective

treatment procedures is required [4]. The methods of treatment might be based on both traditional and cutting-edge technology, depending on the type and severity of the AIE.

The choice of a treatment method is influenced by the ability of streams to self-purify, the allowable pollution levels in water bodies, and the commercial interests of various companies [11]. Decolorization and COD removal from AIE have frequently been accomplished using physical, chemical, and biological approaches. These include chemical precipitation, cation surfactants, electrochemical techniques, reverse osmosis, coagulation, advanced oxidation, membrane separation methods, solvent extraction, filtration electrolysis, biological technology, ultrafiltration, immobilization, and volatilization, among others [12]. Sadly, most of these technologies have drawbacks, including low efficiencies; high initial, operational, and maintenance costs; crud formation; low selectivity and mass transfer rate; high toxicity; operating complexity; large amounts of organic solvents; detrimental to health; high energy demands; production of humongous sludge; low trace metal removal rate; and negative environmental impacts [13]. For decolorization and COD removal from AIE, biosorption-employing bioreactors are the most suitable approach out of all those mentioned due to their accessibility, affordability, simplicity of processing, and high rate of natural affinity to metal ions.

Biosorption process has gained attention recently for the treatment AIE. It has been frequently utilized because of its high operational efficiency, reversibility, reusability, ease of use, quick reaction, selective removal, effective regeneration, and minimized toxic sludge formation. Because of the automated analytical methodologies used, the lack of an emulsion, the high enrichment ratio, and the safety, according to [10], biosorption is the best. The effectiveness of biochar made from agricultural waste as a biosorption material has been evaluated by wastewater professionals [8,9]. Those biotechnological advancements may be advantageous for agro-based enterprises, both as a management strategy and from the standpoint of resource usage in biorefineries [3]. The biochar is a solid, rich in carbon, having a high surface area and great pore structure, and resistant to decomposition and mineralization [14]. Owing to its strong sorption capacity for removing various contaminants from industrial effluents, it has drawn greater attention from researchers recently as a multifunctional material for environmental applications [1]. Biochar creates an excellent support material for biosorbents because of its unique physical and chemical characteristics. However, commercial biochar is expensive. Therefore, building circular economies through agro-waste redirection to achieve environmental sustainability objectives may be possible through the creation of hybrid biosorbents made from agro-waste materials [15].

This study is aimed at treating AIE through combined activated sludge and biosorption processes. The study prepares biochar by combining pulp and paper mill sludge (PPMS) with palm-oil mill-effluent sludge (POMES) that results in hybrid waste sludge biochar (HWSB) for contaminant biosorption. HWSB and AIE are synthesized and characterized. The study uses RSM to optimize the efficiency of CFBS. Finally, decolorization, COD removal, and biosorption biokinetics efficiency for AIE are examined.

2. Materials and Methods

2.1. Materials

The study employed highly pure chemicals and reagents. This includes hydrochloric acid (HCl), sodium hydroxide (NaOH), and buffer powder pillow (sodium phosphate/potassium phosphate) supplied by Avantis Laboratory (Ipoh, Perak, Malaysia). The AIE used was sourced from a local mill in Gurun, Kedah, Malaysia. At this business, biodegradable food packaging materials are created from rice husks and straws. It served as a starting point for the creation of biochar. To avoid affecting the sludge moisture content by the air-drying process, which would have caused the sludge to become anaerobic during the aging phase, the sludge was kept in a well-covered setting. The Malaysian state of Johor's palm oil plant provided the POME sludge. Prior to first characterization, the sludge underwent typical oven-drying to remove extra water.

2.2. Bioreactor Experimental Set-Up and Biomass Acclimation

A 10 L aerobic AIE-fed bench-scale continuous flow bioreactor system (CFBS) was used for the experiment. The bioreactors were attached to a 20 L capacity influent tank via peristaltic pump. Figure 1 shows a schematic representation of the CFBS bioreactor configuration. The CFBS bioreactor was run as-is with the addition of HWSB. Influent AIE was constantly fed into the bioreactors. An air compressor delivered oxygen through a ceramic membrane disperser that was put within the bottom of the bioreactor in order to maintain the dissolved oxygen content at around 80% of the saturation value. The samples were periodically collected, and the bioreactor's functionality was continuously monitored. The pH, COD, and color were constantly measured.
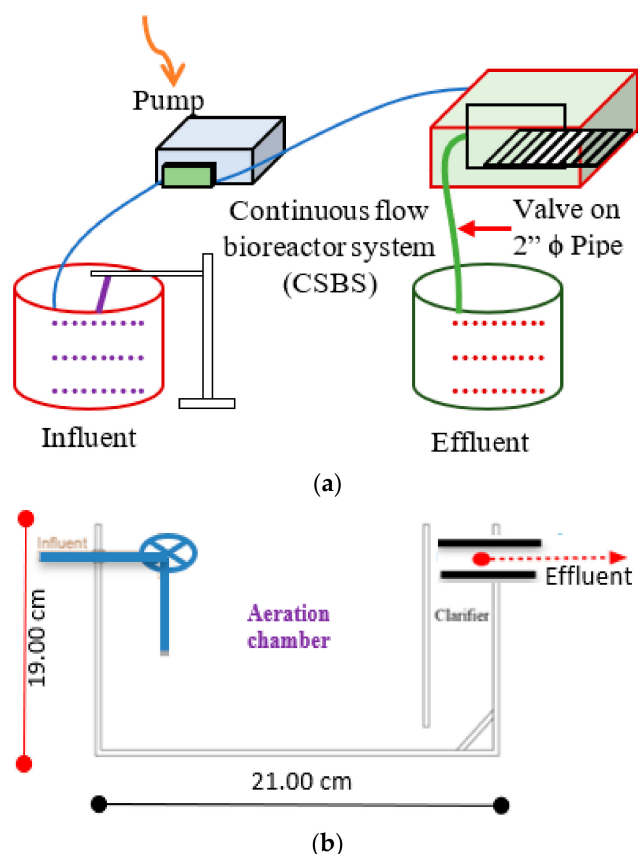

(a)

(b)

Figure 1. Bench-scale schematic diagram of (**a**) full set-up, and (**b**) diagram of main components of CFBS.

The CFBS was inoculated with activated sludge (AS) obtained from the sewage treatment plant (STP) at Universiti Teknologi PETRONAS (UTP), Perak, Malaysia. The characteristics of the AS are highlighted in Table 1. Prior to the commencement of the experiment, the AS was aerated for 3–7 days.

Table 1. STP's activated sludge characteristics.

Parameter	Mean Value
pH	7.14
Temperature (°C)	27.42
TS (mg/L)	10,376
SS (mg/L)	8205
MLVSS/MLSS	0.87
Settleability (ml/L)	244.91
SVI (mL/g)	99.76

2.3. HWSB Synthesis

The acquired PPMS and POMES used to make biosorbents were dewatered, and the leftover material was then dried by air for 48 h before being roasted to dryness in an oven for 24 h at 105 °C [13]. A 1:1 weight ratio of PPMS and POMES was used to create the biosorbent material. After being agitated for an hour in an ultrasonic bath, the mixture was dried overnight in an oven at 105 °C. One hundred grams of the dry material was firmly packed within a tube with a diameter of 5 cm and a length of 25 cm to pyrolyze the mixture (PPMS/POMES). For the purpose of positioning the PPMS/POMES, glass wool was applied to both ends of the device. To rid the tube of oxygen prior to pyrolysis, the sludge sample mixture in the tube was purged with nitrogen for 5 min. The tube was afterward sealed and placed inside a furnace [8]. To make biochar, the furnace temperature was set to rise 10 °C/min over the course of two hours until reaching 800 °C. The final biochar (HWSB) was then allowed to cool at ambient temperature while being surrounded by nitrogen gas. It was then washed with 1.2 M HCl and subsequently rinsed with distilled water until the pH was neutral [16]. Then, it was dried for 24 h in an oven at 105 °C. Prior to use, the HWSB was kept in sealed polypropylene sachets after being crushed, powdered, and sieved to a particle size less than 150 μm.

2.4. HWSB Characterization

To characterize the HWSB, X-ray fluorescence spectrometry was used to evaluate the components and specific surface area was determined. A Zeiss super 55 VP instrument (Carl-Zeiss AG, Oberkochen, Germany) was used for field emission scanning electron microscopy. HWSB was ground and mixed with spectrally pure KBr at a ratio of 1:100, and it was pressed into a translucent sheet under a certain pressure. Fourier transform infrared (FTIR) spectra were recorded using a FTIR spectrometer (NICOLET iS10, Thermo Scientific, Waltham, MA, USA) in the 400–4000 cm^{-1} range, and the detector resolution was 4 cm^{-1} at 100 cycles.

2.5. Analytical Methods

The *Standard Methods for the Examination of Water and Wastewater*, and the analytical procedures and laboratory tools described therein, were used in this study (American Public Health Association, Washington, CA, USA). The DRB200 Reactor was used to digest the AIE in order to measure the COD values in the influent and effluent samples. The HACH DR3900 spectrophotometer was used to measure COD and color absorbance. A HACH SensIONTM pH meter set was utilized for pH measurement. All measurements were in triplicate and the CFBS performance efficiencies recorded.

2.6. CFBS Process Optimization by RSM for COD and Color Removal

The steps involved in optimizing the RSM approach were as follows: select independent variables and a potential response; select an experimental design strategy; carry out experiments and obtain results; fit the model equation to experimental data; obtain response graphs and model verification (ANOVA); and, finally, choose the optimal conditions. The RSM employed in this investigation was a CCD with two independent variables: AIE concentration and HRT. Using Design Expert software (11 trial versions, Stat Ease, Minneapolis, MN, USA), the design matrix was examined [6] and the optimization was carried out to increase the elimination of COD and color. The effects of AIE concentration on the removal of COD and ammonia were examined in the current work using a typical CCD design with two variables. Eleven tests were carried out. Table S1 provides the CCD for the variable in the specified range and level in terms of coded and real words; the outcomes were then examined further [17]. Two dependent parameters, namely COD and color removal, were evaluated as responses to achieve the ideal AIE concentration and HRT.

2.7. Models for Substrate Removal Biokinetic Analysis in CFBS System

2.7.1. First-Order Kinetic Model

In steady-state settings, when first-order kinetics is assumed to be dominant, the rate of change in substrate concentration in CFBS can be expressed by Equation (1), as follows:

$$\frac{S_{in} - S_{ef}}{\tau} = k_1 \, S_{ef} \tag{1}$$

By plotting $(S_{in} - S_{ef})\,/\tau$ versus S_{ef}, the value of k_1 can be calculated using the line's slope.

2.7.2. Grau Second-Order Kinetic Model

The model's general equation can be expressed using Equation (2):

$$-\frac{dS}{dt} = k_s \, \chi \left(\frac{S_{ef}}{S_{in}} \right)^2 \tag{2}$$

By integrating Equation (2) and then linearizing it, Equation (3) can be obtained:

$$\frac{S_{in}\tau}{S_{in} - S_{ef}} = \tau - \frac{S_{in}}{k_s \, S_{ef}} \tag{3}$$

where k_s = second-order contaminant removal rate constant, $(1/d)$; $(S_{in} - S_{ef})/S_{in}$ reflects the efficacy of pollutant removal. It is denoted as ε. Nevertheless, Equation (4) occurs if the second factor of the right section of Equation (3) is regarded as an allowable constant:

$$\frac{\tau}{\varepsilon} = c + d \tag{4}$$

The slope and intercept of the line are generated by plotting $\frac{\tau}{\varepsilon}$ versus τ, where the amount of c and d are constant values.

2.7.3. Modified Stover–Kincannon Model

Kincannon and Stover developed a model based on the premise that the rate of substrate consumption is proportional to the rate of organic loading [18]. The modified Stover–Kincannon model can be summarized as follows:

$$\frac{dS}{dt} = \frac{Q}{v_R} \left(S_{in} - S_{ef} \right) = \frac{U_{msr} \left(\frac{QS_{in}}{v_R} \right)}{K_v + \left(\frac{QS_{in}}{v_R} \right)} \tag{5}$$

Equation (5) can be linearized to produce Equation (6):

$$\left(\frac{dS}{dt} \right)^{-1} = \frac{v_R}{Q\left(S_{in} - S_{ef} \right)} = \frac{K_v}{U_{msr}} \left(\frac{v_R}{QS_{in}} \right) + \frac{1}{U_{msr}} \tag{6}$$

By plotting $\frac{v_R}{Q\left(S_{in} - S_{ef}\right)}$ versus $\frac{v_R}{QS_{in}}$, the slope and intercept are equal to $\frac{K_v}{U_{msr}}$ and $\frac{1}{U_{msr}}$, respectively, where U_{msr} = maximum contaminant removal rate (g/L d) and K_v = saturation value constant (g/L d).

3. Results and Discussion

3.1. AIE Characteristics

The AIE were subjected to a physicochemical examination, which revealed that it has significant contamination parameters. The properties of AIE contaminants revealed a high pH possibly caused by NaOH and Na_2S residues remaining from the pulping process [19]. The concentrations for the influent AIE characteristics as obtained were 7.63 ± 0.0655 pH,

26.1 ± 0.3728 °C, 1087 ± 24.9933 total dissolved solids (TDS), 709 ± 10.1980 total suspended solids (TSS), 61.9 ± 2.7580 NH_4^+-N, 0.48 ± 0.0245 nitrate, 154 ± 4.8990 total phosphorus (TP), 5327 ± 6.6833 COD, 1547 ± 7.1180 BOD_5, (mg/L); 1996 ± 2.4495 Pt.Co., 178 ± 2.1602 nephelometric turbidity units (NTU). However, the concentrations of organic matter and nutrients in the wastewater were higher than the permissible levels. It could be observed that AIE has a high percentage of solids. The high COD concentration in the AIE discharges could be resulting from the presence of high molecular weight chemical molecules [20]. The high color concentration in the effluent increased the toxicity of the effluent [21].

3.2. HWSB Analysis Result

3.2.1. Oxide Composition, Elemental Analysis, and Physical Properties of HWSB

The biosorbent chemical composition is 23.38% SiO_2, 15.62% Al_2O_3, 9.63% SO_3, 10.28% CaO, 2.17% Fe_2O_3, 2.04% MgO, 0.88% MnO, 0.91% P_2O_5, 0.63% K_2O, 0.87% Cl, 0.52% others, and a 33.07% LOI. The HWSB studied in this study shares some chemical characteristics with them. Table S2 lists the measured elemental composition of the HWSB. The main components discovered to be present were Si, Al, C, O, K, and Cl. The high concentration of Si and C observed in HWSB was caused by the presence of agro-industrial waste sludge; all facilitated the formation of pores and, therefore, the process of biosorption. Table 2 highlights the pH, surface area, pore volume, radius, and size. The HWSB was discovered to have larger specific surface area, more pores, and less surface-oxygen-containing functional groups. Thus, its biosorption capacity became higher. The HWSB falls under the mesopores category of materials. The HWSB's enormous surface area may be related to the thermal processing it undergoes and the type of waste biomass materials used. These two causes caused a progressive increase in the hybrid material's mean pore size.

Table 2. HWSB surface and structural properties.

Parameter	Values
pH	7.48
BET surface area (m^2/g)	327.09
Total pore volume (cm^3/g)	0.462
Mean pore radius (Å)	85.10
Mean pore size (nm)	1.903

3.2.2. FESEM

In Figure 2, the micrographs of the HWSB surface morphology after pyrolysis (a and b) are depicted. Energy dispersion spectroscopy was used to evaluate the image, which was captured at a magnification of 1000–5000 times (EDS). The HWSB surface morphology demonstrated that it was best used as a biosorbent to create microscopic cavities and a loose spore-like surface. The FESEM also showed an unusual interconnected porous nanoflake structure. The mesoporous slits between the adjacent nanoflakes were also demonstrated [22]. The HWSB showed a sieve-like structure with uneven and remarkably porous holes and lettuce-shaped honeycomb surfaces that were unlikely to combine into potentially contaminant-trapping aggregates. This was evidence that the pretreatment removed external fibers, increased surface area, and made cellulose accessible to enzymes [23]. Given their free-flowing nature and sharp edges, the HWSB particles readily gathered to form porous and loose materials. The extremely small quantity of calcite that was found in the matrix may have resulted from a CO_2 and CH side reaction that occurred when handling the sample. In addition, there were still vacant areas in the matrix that could be used for the deposition of fresh hydration products [24].
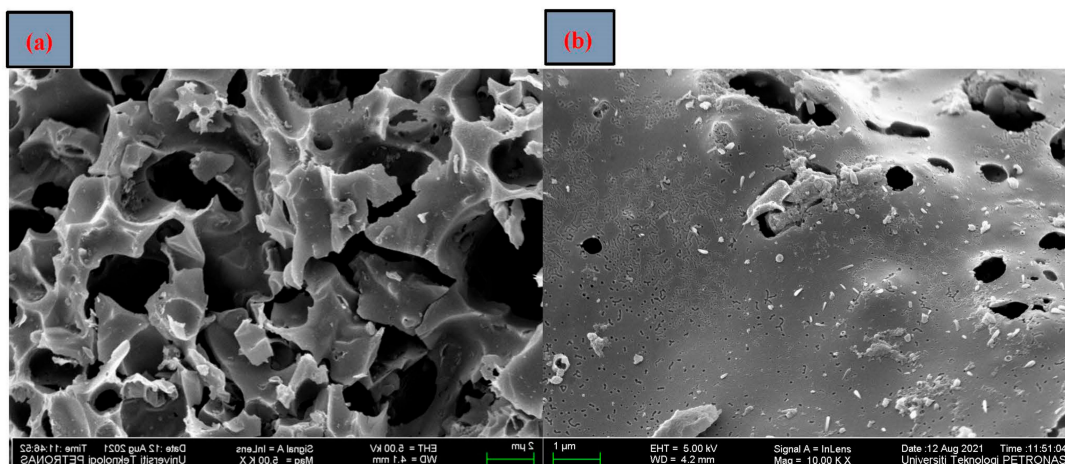
Figure 2. FESEM electron images at (**a**) 2 μm, (**b**) 1 μm for HWSB.

3.2.3. FTIR

The FTIR spectra of the HWSB biosorbents are shown in Figure 3. It has bands at different heights: 3435.18, 1632.37, 1053.41, 832.15, 777.35, 564.67, and 460.46 cm^{-1}. =C-H, C-OH, C-O, Si-O, C=C, and C=O, were the functional groups and stretches that were visible on the surface of HWSB, and they comprised either positively or negatively charged ions [25]. The presence of =C-H stretch on the surface of the material was confirmed by the peak at 3435.18 cm^{-1}. The presence of the peak at 1632.37 cm^{-1} would indicate that the aldehyde or ketone had undergone carbonyl (C=O) stretching, which results in the creation of additional C=O and C-O functional groups. The presence of alcoholic groups created a broad biosorption band in the HWSB sample at about 1053.41 cm^{-1}. This was caused by the depolymerization of the lengthy polymeric chain of the raw material [26]. The C-H bend is designated to be the cause of the biosorption bands from 564.67 to 832.15 cm^{-1}. The presence of quartz (Si-O) functional groups is indicated by the biosorption peak at 460.46 cm^{-1}, which is primarily brought on by aromatic-carbon–carbon rocking vibrations [27]. The biosorption of COD and color was mostly caused by the carboxyl and hydroxyl functional groups.
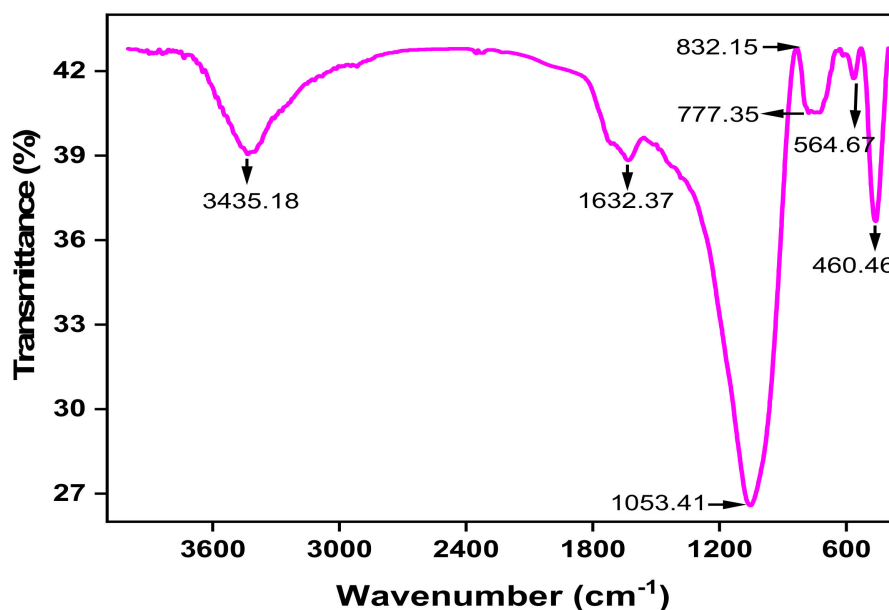

Figure 3. FTIR spectra of HWSB after exposure to elevated temperatures.

3.2.4. Proximate and Ultimate Analysis

To identify the HWSB chemical components prior to being used in the CFBS for AIE treatment, the study investigated its pH and also performed ultimate and proximate analysis. The proximate analysis was done promptly, and it offers a prediction of how burning biomass would behave [28]. Results are shown in Table S3. The labile and stable components of chars are represented by the VM and FC contents, respectively [29]. HWSB has extensive ash, VM, and FC. This can lead to obtaining a high calorific value. The resultant composite's inorganic character was further demonstrated by its high carbon content and high percentage of volatiles. The volatile matter from the meso-carp fiber and alum sludge biochar may have been converted into FC during the carbonization process, which could account for the high value for the FC [30]. The significant amount of ash demonstrated the material's effectiveness as an excellent biosorbent [31]. The high ash content can be attributed to the retention of mineral components and loss of volatile materials. The carbonization of the two biomass waste materials used in this study, according to the results of the proximate analysis, improved the quality of the composite that was created. Even though the volatile component was significant, part of it is claimed to have been turned into gaseous products, and the HWSB had a considerable amount of ash. The existence of much ash suggests poor combustion and longer burning times. The durability of the biosorbent, which has a high SiO_2 content, 23.38%, has been amply demonstrated. To determine the elemental compositions, the HWSB was subjected to the final analysis, the results of which are shown in Table S3.

3.3. Effect of AIE Concentration and HRT on COD and Color Removal
3.3.1. COD Removal

It is generally known that the majority of organic compounds, especially the soluble compostable portion, are removed at the start of the reaction stage [32]. The effects of HRT on the nitrification and denitrification processes are complex. The initial quantity of nitrogen components found, HRT, biological floc volume, aeration rate, quantity, and properties of the underlying organic substances are a few of the most important and valuable aspects on these processes [12]. Figure 4 shows the profiles of influent and effluent COD concentrations together with COD removal effectiveness in the CFBS. The data showed that the COD elimination rate fluctuated over the course of acclimation for about two weeks. Afterward, a little fluctuating steady state condition was achieved. Because at a higher HRT, the level of aluminum's anodic dissolution rises, leading to the production of more precipitate and the removal of organics, COD removal efficiency rose steadily after the addition of HWSB to the CFBS. During the first nine days of operation, the CFBS showed a quick COD elimination rate with just a small amount of volatility, and after that, a distinct steady state condition was noticed. Furthermore, the HRT showed effective COD elimination capabilities. Numerous investigations have demonstrated that the clearance efficiency typically declines significantly as the HRT increases. Additionally, they stated that the low biodegradability of industrial effluents is confirmed by the low removal efficiency (≤20%) of COD. Poor elimination of COD and color was the outcome of the treatment of low biodegradable AIE. However, the removal efficiency was significantly improved by mixing HWSB with CFBS. The maximum removal efficiency in this investigation was 76.52%, with the average removal efficiency of COD in the CFBS being around 69.85%. According to the study's findings, the CFBS-HWSB performed relatively better in terms of stability than other biosorbents. This might be explained by the notion that some biosorbents might be somewhat less conducive to the suspension of biomass and the biosorption of contaminants. Comparatively, a study by [33] showed that a consistently fed bioreactor with virgin car wash wastewater achieved a peak COD removal efficiency of 87%. The outcomes were notably better than the COD removal efficiency of 73.9% that was reported by [34] for the biotreatment of car wash wastewater coupled with energy production in a hybrid treatment unit.
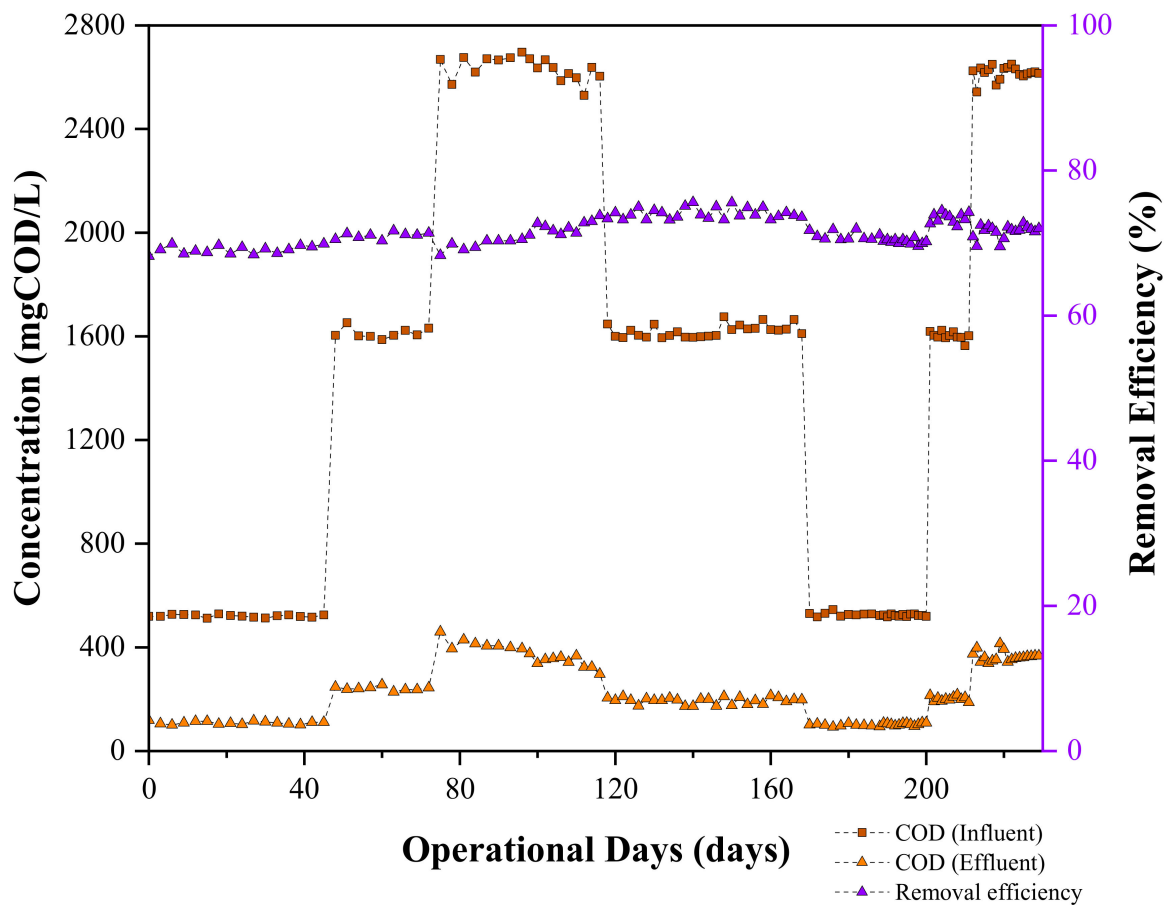
Figure 4. The experimental time course of CFBS in terms of COD concentrations and removal efficiency.

3.3.2. Color Removal

Color is also considered an organic contaminant in AIE. As a result, it is critical to monitor how this element declines and is eliminated. Various writers have also found a decrease in the color of AIE, although very few investigations have been tailored to environmental and dietary circumstances [35]. According to the literature, AIE decolorization may be significantly aided by sodium nitrate, an inorganic nitrogen source [36–38]. Ammonium nitrate, on the other hand, may contribute negatively to color reduction (the inorganic nitrogen source) [15]. The process of color change may also be affected by the reduction in culture medium since the inoculum size may become even larger [39]. The color removal efficiency profiles during the course of 229 days of uninterrupted operation are shown in Figure 5. The minimum and maximum color removal efficiencies achieved by CFBS were 52.71% and 66.97%, respectively. Compared to testing during the acclimatization phase, at the same operational conditions, HWSB addition to the bioreactor offered significantly higher removal efficiency, which signifies the role of HWSB in color removal. In the HWSB-CFBS, ideal removal effectiveness was achieved at a 30% AIE concentration and 2 d HRT. At low HRT, maximum removal efficiencies were often attained. Higher HRT resulted in lower removal efficiency. The results obtained from the HWSB-CFBS treatment system demonstrated that the elimination of color was caused by biosorption and biological phenomenon [40]. The biosorbent (HWSB) has superior ability for removal of several dissolved organic pollutants from AIE due to its high surface area, hydrophobic surface, and broad variation in pore sizes. The results obtained from the HWSB-CFBS were equivalent to the color removal efficiency of 61.93% obtained by [41] for the treatment of paper mill effluent.
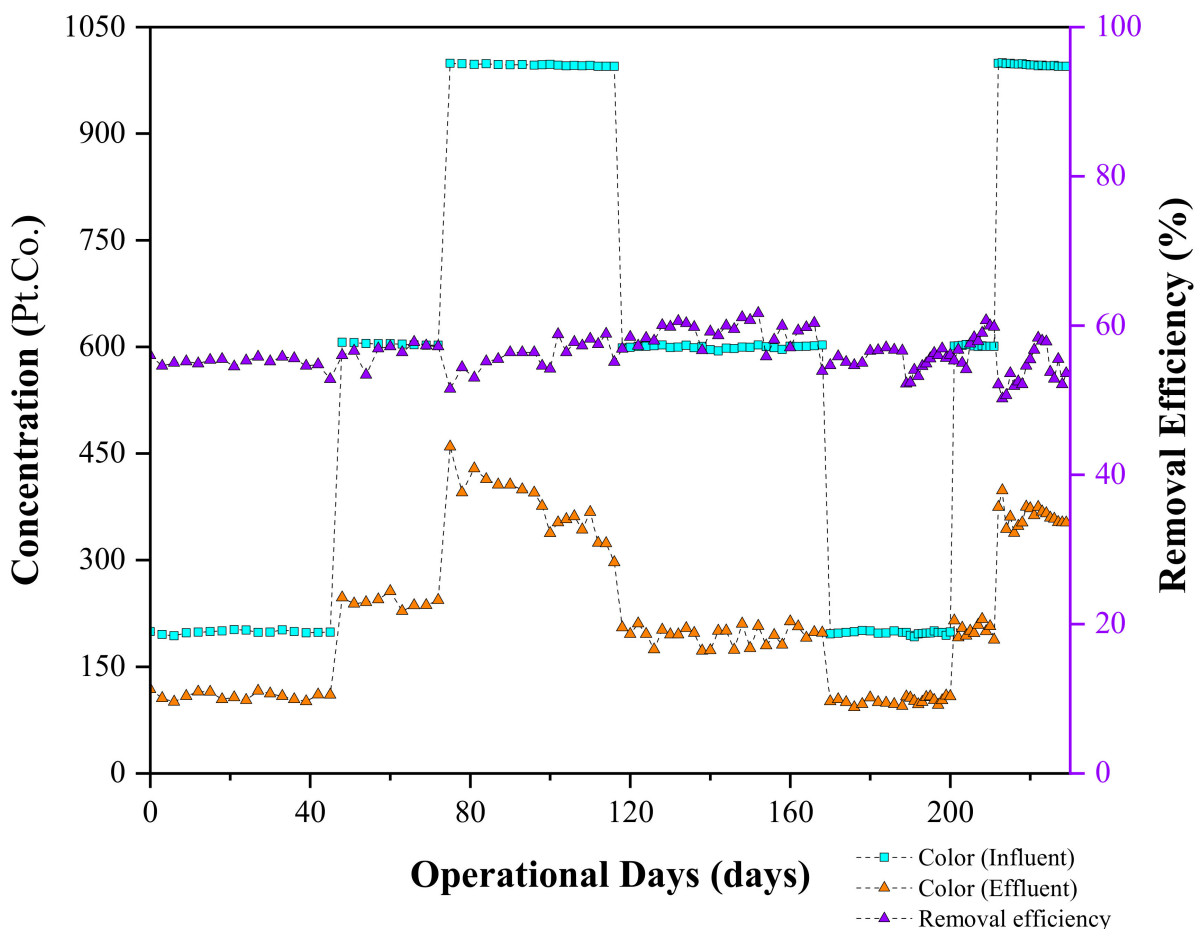
Figure 5. The experimental time course of CFBS in terms of color concentrations and removal efficiency.

3.4. Optimization by RSM

3.4.1. Model Fitting and Statistical Analysis

The CCD of RSM was used to refine the parameters for optimum COD and color biosorption on HWSB. The range (high and low) of the two variables examined was selected, and the maximum percentage elimination of COD and color was sought as depicted in Table S4. The levels of these independent variables in terms of coded factors are shown in Table S5. In the bench-scale CFBS, AIE treatment was carried out. RSM was used to assess the experimental data and create an empirical model of the responses [42]. The polynomial equations obtained for COD and color reduction are presented in Equations (7) and (8) for CFBS, as follows:

$$\text{COD removal (\%)} = +72.52 - 5.33A - 3.80B + 1.92AB - 7.07A^2 - 1.96B^2 \qquad (7)$$

$$\text{Color removal (\%)} = +64.92 - 1.95A - 1.37B + 1.14AB - 8.99A^2 + 0.3163B^2 \qquad (8)$$

where A and B are the coded values of the test variables, AIE (A) and HRT (B).

The best conditions were attained at 30% AIE concentration and a 2-day HRT for the largest percentage of COD and color elimination. The maximum COD and color removal at these optimal circumstances was estimated to be 76.52% and 66.97%, respectively. In Table 3, which represents the modified model equation in terms of coded and real components, the final equation derived for COD and color elimination is given in terms of actual factors.

Table 3. Final equation in terms of actual factors for CFBS.

COD Removal	=	Color Removal	=
+70.11561		+55.01228	
+0.602719	AIE	+1.13805	AIE
+1.15640	HRT	−4.33443	HRT
+0.096000	AIE × HRT	+0.056750	AIE × HRT
−0.017684	AIE^2	−0.022484	AIE^2
−1.95868	HRT^2	+0.316316	HRT^2

3.4.2. Three-Dimensional Response Surface Plots

Three-dimensional response surface plots for the measured responses were created to better understand the effect of independent factors and their relationships on the dependent variable [43]. Figure 6a–d show the % COD and color removal as a function of AIE concentration and HRT as 3D response surface plots. The curved part of the 3D figure indicates that the elimination of COD and color were discovered to have an almost positive interaction effect on these two variables. The elimination of COD and color in this study increased as AIE concentration grew (from 10% to 30%) with an increased HRT from 1 to 2 days. However, as AIE concentration climbed further (to 50%), the removal of COD and color began to decline. This could be because of the small number of biosorption sites [20].
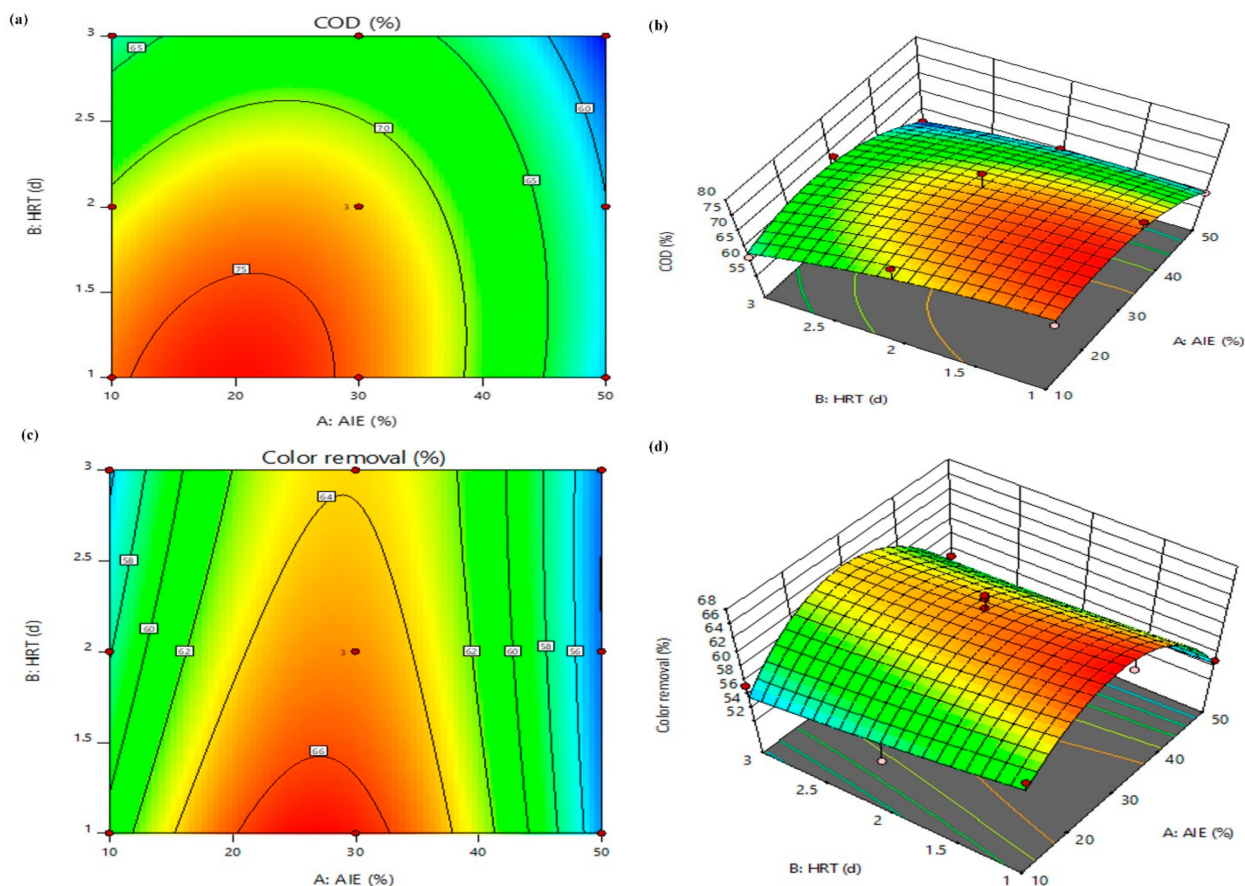

Figure 6. Contour and surface plot for the removal of (**a**,**b**) COD and (**c**,**d**) color from the CFBS system.

In this investigation, when a circular 3D response of the surfaces was discovered, the interaction between the related variables was minimal. The pattern of the surface curves demonstrates how the variables interact. The HRT sharp curve indicates that COD was highly susceptible to this issue. The perturbation plot displays how the factors' relative influences on the response vary. The elliptical shape of the contour in each graph represents

how all the variables interact with one another [44]. The surface contained in the smallest ellipse in the contour diagrams indicates that there was a maximum projected drop in COD and color. Figure 7 displays the plots of all the projected values of the answers versus their actual values (a–d). The figure demonstrates that there was a strong correlation amongst the experimental and predicted values in the plots' ranges for all the sites along the straight line.
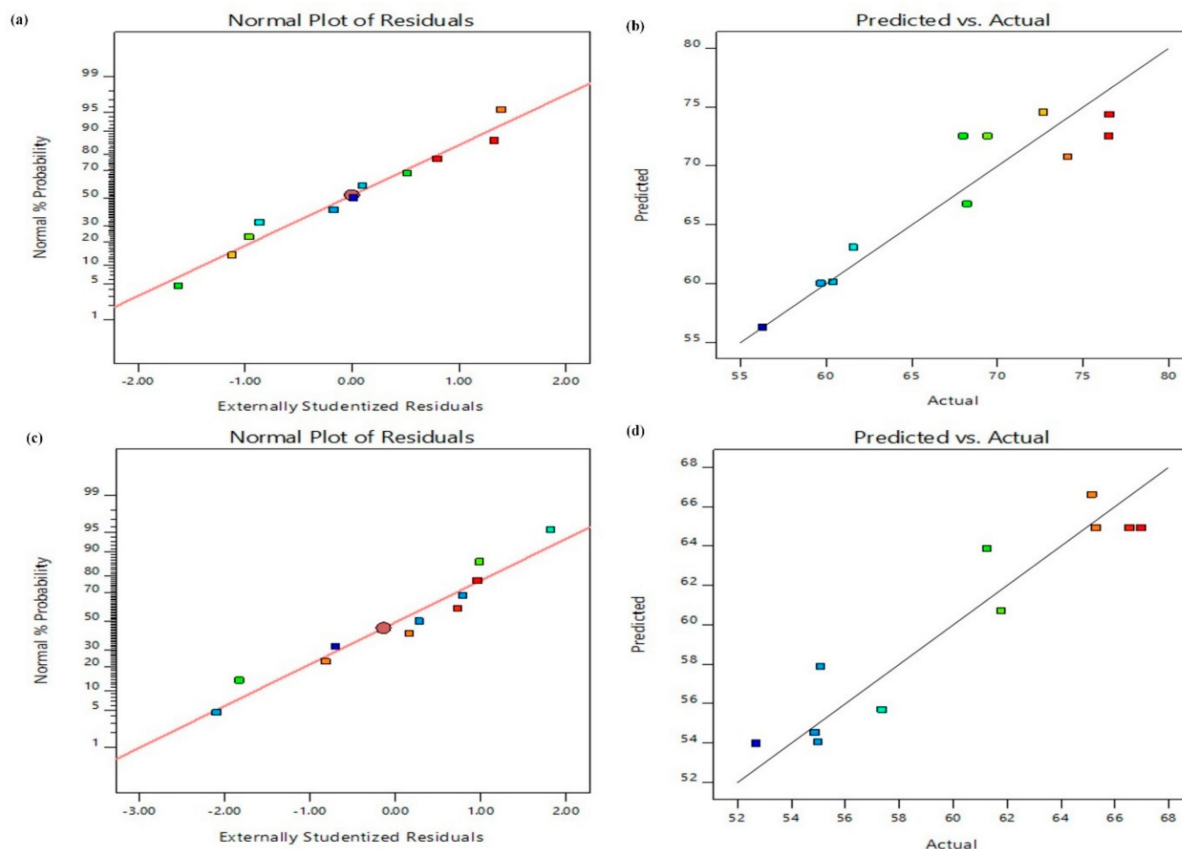

Figure 7. Plots of residuals and predicted versus actual plots of CFBS for COD (**a**,**b**) and color (**c**,**d**) removal.

3.4.3. Analysis of Variance (ANOVA)

Table 4 displays the ANOVA for the projected response-surface quadratic model without the nonsignificant model terms. The table provided the F value and accompanying *p* values. For COD and color decrease, the Fisher/model F-values for all regressions were high. Large values of F show that the model was significant, and the regression equation can explain most of the response variation [45–47]. The quadratic regression model's ANOVA shows that it is significant.

In the CFBS bioreactor, the model F-values of 6.33 and 8.47 confirm that the model is significant, and for the elimination of COD and color, respectively, there is only a 3.20% and 1.75% chance that an F-value this large could occur owing to noise by experimental errors. The significance of the model terms is shown by the values of "Prob > F" 0.0500. In this instance, the terms for the removal of color are A, B, and A^2, while A is the only important model term for the removal of COD.

If the result is more than 0.1000, the model terms are not significant. The lack-of-fit F-values for COD and color elimination, respectively, are 0.46 and 12.73, which indicate that the lack of fit is not significant in comparison to pure error and that there is a 74.06% and 7.37% possibility that noise might be the cause of such a huge lack-of-fit F-value. The reduction ramps and desirable COD and color removal solution produced by a design professional utilizing modeled parameters following optimization are shown in Figure 8.

The optimization ramp for AIE concentration and HRT shows the desirability of the independent variables. Therefore, if the value is more than 0.1000, each dot on the ramp indicates the targeted variable and response behavior target [48].

Table 4. ANOVA by RSM for COD and color removal efficiencies in CFBS.

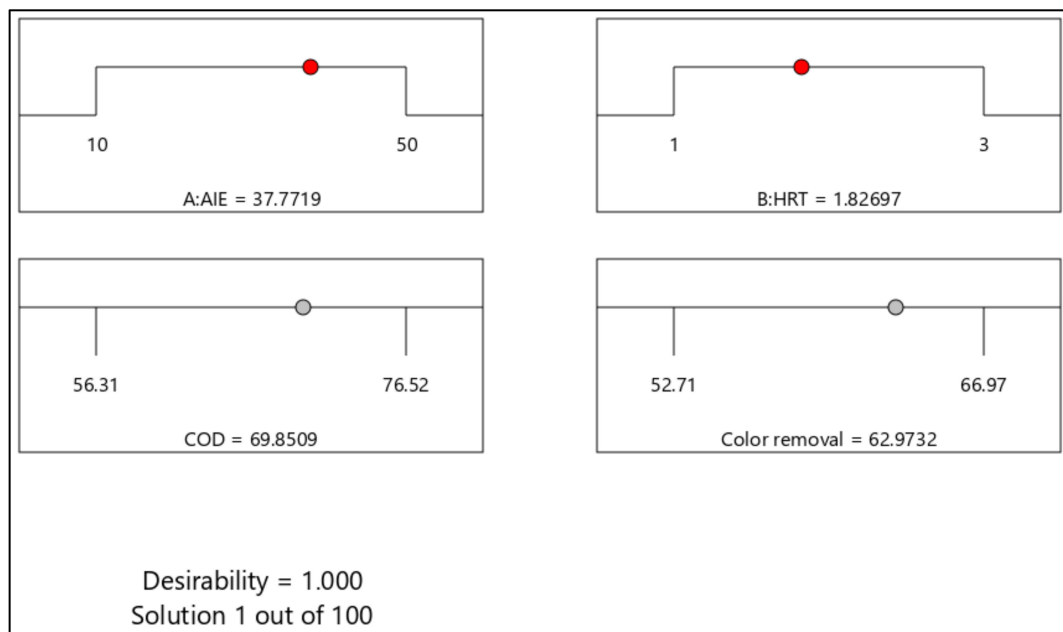|	Sum of Squares	df	COD Mean Square	F-Value	p-Value	
Model	438.63	5	87.73	6.33	0.0320	significant
A-AIE conc.	170.24	1	170.24	12.29	0.0172	
B-HRT	86.56	1	86.56	6.25	0.0545	
AB	14.75	1	14.75	1.06	0.3495	
A^2	126.76	1	126.76	9.15	0.0292	
B^2	9.72	1	9.72	0.7017	0.4404	
Residual	69.25	5	13.85			
Lack of Fit	28.17	3	9.39	0.4570	0.7406	not significant
Pure Error	41.09	2	20.54			
Cor Total	507.89	10				
	Sum of Squares	df	Color Mean Square	F-Value	p-Value	
Model	255.91	5	51.18	8.47	0.0175	significant
A-AIE conc.	22.81	1	22.81	3.78	0.1096	
B-HRT	11.21	1	11.21	1.85	0.2314	
AB	5.15	1	5.15	0.8527	0.3982	
A^2	204.91	1	204.91	33.91	0.0021	
B^2	0.2535	1	0.2535	0.0419	0.8458	
Residual	30.21	5	6.04			
Lack of Fit	28.71	3	9.57	12.73	0.0737	not significant
Pure Error	1.50	2	0.7519			
Cor Total	286.12	10				

A:AIE = 37.7719

B:HRT = 1.82697

COD = 69.8509

Color removal = 62.9732

Desirability = 1.000
Solution 1 out of 100

Figure 8. Optimization desirability in ramps for the CFBS system.

3.4.4. Fit Statistics

The model fit summary for the quadratic model for both pollutants is shown in Table 5. R^2 was found to be higher than 0.86 for both responses. This suggests that the experimental data's prediction was very accurate [49]. Typically, the higher the CV number is, the more reliable the experiment [42]. Here, a higher value of CV (>4) for the two replies denotes a sufficient signal and improved experiment reliability, both of which are desired. The COD and color present ratios of 6.6400 and 6.9550, respectively, suggesting a sufficient signal. The design space can also be explored using this technique [50].

Table 5. Fit statistics.

	COD	Color
Std. Dev.	3.72	2.46
Mean	67.59	60.19
C.V. %	5.51	4.08
R^2	0.8636	0.8944
Adjusted R^2	0.7273	0.7888
Predicted R^2	0.4222	0.2790
Adeq. precision	6.6396	6.9549

The statistics for model comparison are described in Table 6. When all other factors are maintained constant, the anticipated adjustment in response for each corresponding change in factor value is shown by the coefficient estimates in Table S5 In an orthogonal design, the intercept is the mean response over all runs [51–54]. The coefficients alter the average in its vicinity depending on the factor values. The VIFs are 1 when the factors are orthogonal. The VIFs are greater than 1 when the factors are multicolinear. The severity of the link between the components increases with the VIF. In general, VIFs < 10 are acceptable.

Table 6. Model comparison statistics.

	COD	Color
PRESS	293.44	206.29
−2 Log Likelihood	51.46	42.33
BIC	65.84	56.72
AICc	84.46	75.33

3.5. Biokinetic Models for AIE Treatment in the CFBS

3.5.1. First-Order Model

In essence, the first-order kinetic model depicts how changes in HRT affect system efficacy. Trying to orchestrate the average specific substrate removal rate against the average effluent COD in this study, which matched the bioreactor's organic matter removal biokinetics, allowed for the determination of the slope of the graph (k_1). Upon calculating the first-order biokinetic model coefficients k_1 and R^2, the slope of the line at steady-state was used to plot $(S_{in} - S_{ef})/\tau$ and S_{ef} in Equation (1). As seen in Figure 9, the relationship between $(S_{in} - S_{ef})/\tau$ and S_{ef} created a straight line. The k_1 and R^2 constants for COD elimination in the CFBS were discovered to be 2.5836 and 0.2024, respectively. The first-order model seems unable to effectively forecast COD elimination efficiency, as evidenced by the low R^2 values for the CFBS. As a result, it cannot be administered with sufficient precision. The degrading capacity of the microorganism increases with increasing k_1 values [55]. However, first-order kinetics had a low k_1 value. The first-order model constant in the current study was tiny, but it was nevertheless higher than the figures provided by several other studies. Variations in operating conditions and effluent type may be the cause of variations in k_11 levels. The AIE used as feed was substantially more biodegradable, as seen by the higher k_1 values. As a consequence, the experiment's findings do not support this theory. This indicates that the biokinetics of CFBS could not be entirely

or partially explained by the first-order model. These findings agree with those of [29], who estimated k_1 to be 1.09 per day with a correlation coefficient of 0.521. Similar to this, a study by [56] produced coefficients of 1.135 and 0.24 for k_1 and R^2, respectively, after constructing first-order graphs. As a result, the model's performance in terms of R^2 was outstanding. This might be a result of the study's consideration of several other operating parameters.
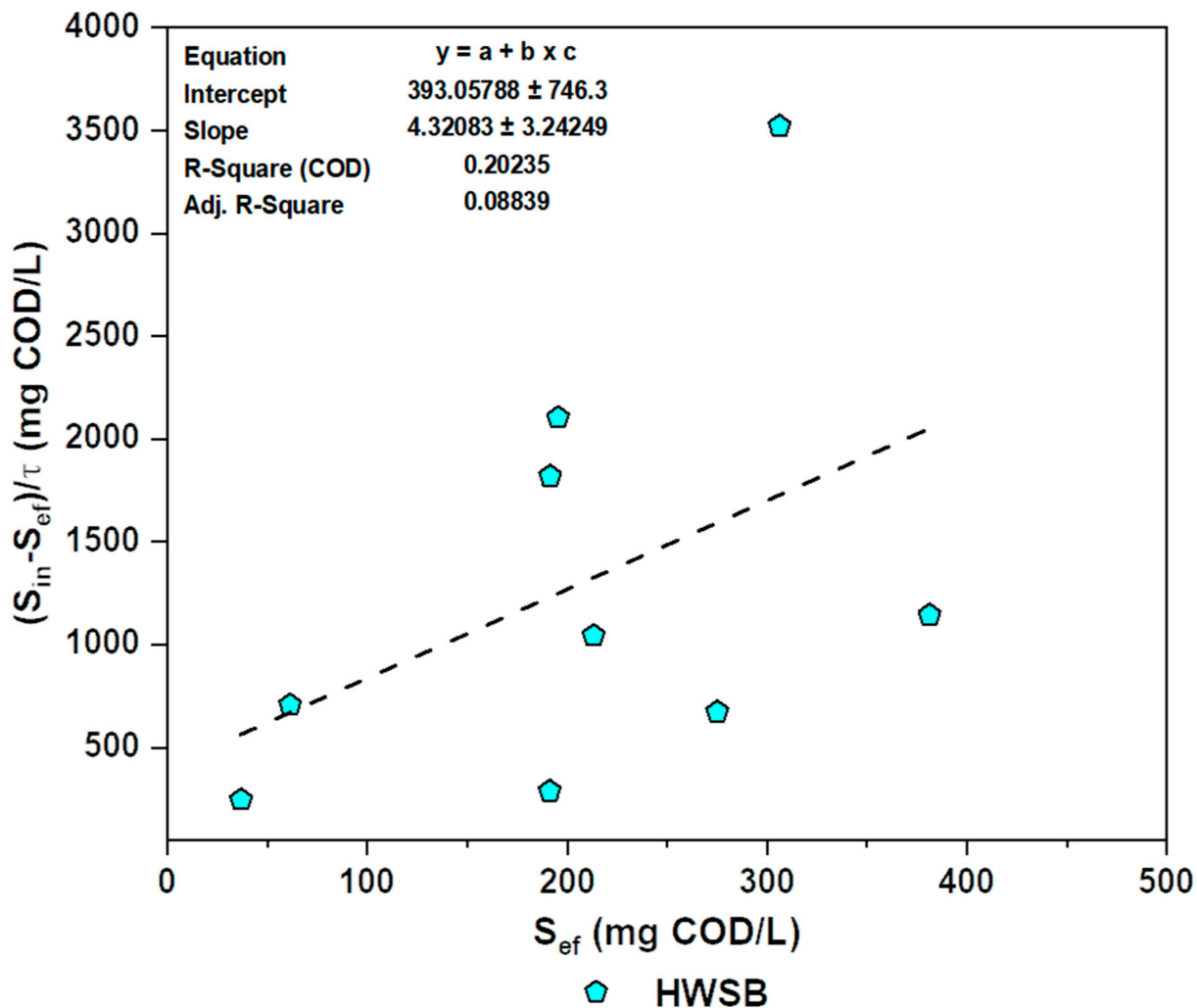

Figure 9. First-order kinetic plot of COD for CFBS.

3.5.2. Modified Stover–Kincannon Kinetic Models

Throughout this work, the biokinetic coefficients were calculated by plotting $\frac{v_R}{Q(S_{in}-S_{ef})}$ versus $\frac{v_R}{QS_{in}}$ (see Figure 10). The coefficients are essential in determining how much wastewater and how fast a bioreactor can process it. The coefficients obtained can also be used to determine the amount of CFBS needed to produce the desired concentration of effluent substrate. The relationship between loading rate and particular substrate utilization rate for each concentration is shown as a straight line in Figure 10. The saturation value constant (K_v) and maximum utilization rate (U_{msr}) for COD removals were calculated from the line indicated on the graph. The R^2, K_v, and U_{msr} values for COD in the CFBS were, respectively, 0.9741, 185.3 g/L.d, and 0.8971 g/L.d. Numerous AIE have been discovered to be applicable to the model total loading technique. The high Kv value shows that the CFBS managed the AIE extremely well. The UAF used has limited capability in handling high-strength effluent, nevertheless, as evidenced by the low value of K_v obtained by [57]. The close values between U_{msr} and K_v indicate that system efficiency decreases as the organic loading rate increases. The Stover–Kincannon model was used to forecast the behavior and design

of the upflow aerobic immobilized biomass (UAIB) reactor [34]. The measured values of K_v and U_{msr} were 106.8 g/L/d and 101.0 g/L/d, respectively. These data show the highest substrate removal by aerobic organisms versus time and the substrate removal by microorganisms through time.
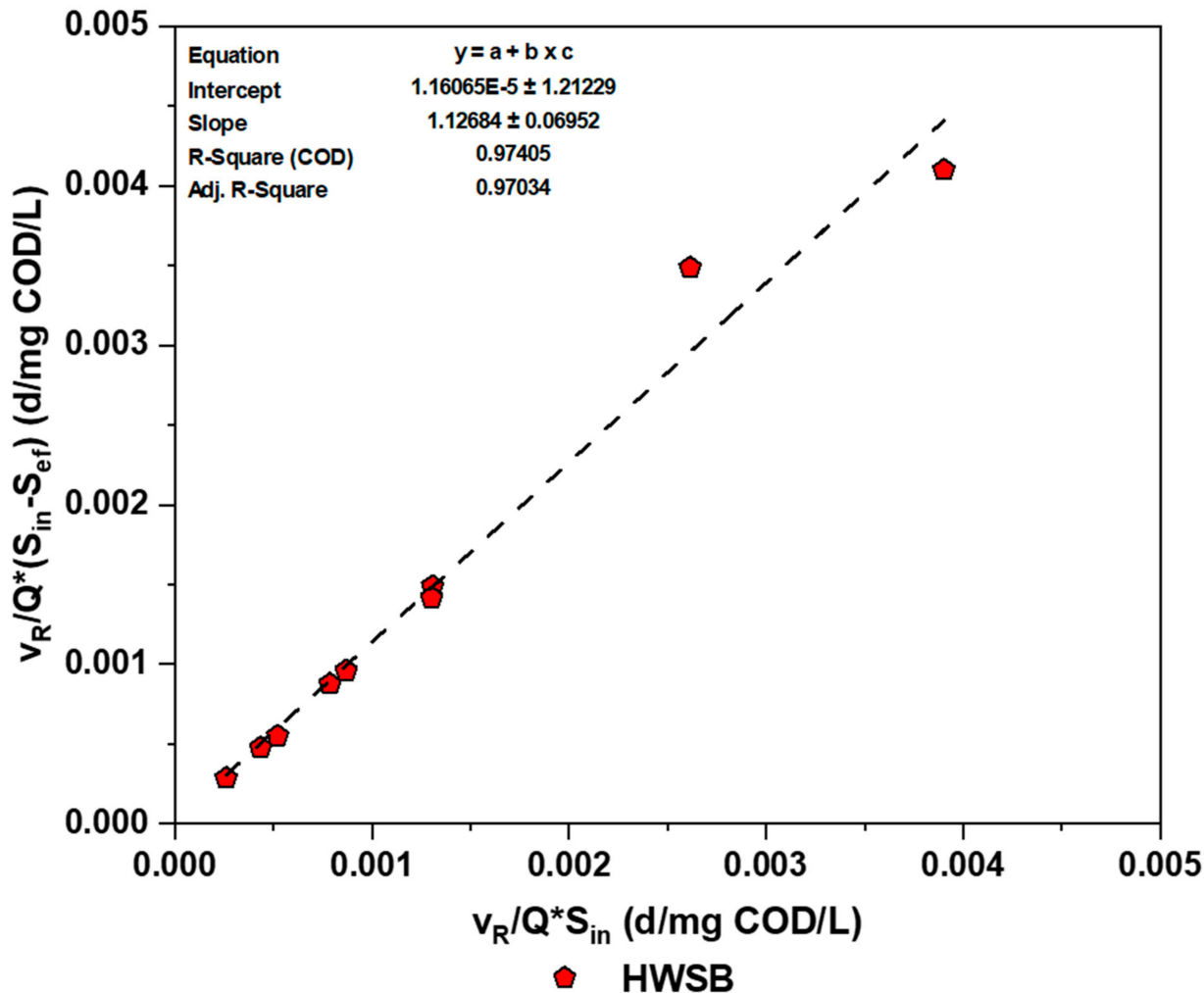

Figure 10. Modified Stover kinetic plot of COD for CFBS.

3.5.3. Grau Second-Order Model

Output of the evaluation using Equation (4) is displayed in Figure 11 and used to determine the biokinetic coefficients. The slope and intercept of the straight line were used to calculate c and d, respectively. For COD elimination in CFBS, the c and d values were 0.1075 per day and 1.1625, respectively. The biomass concentration in the CFBS and the influent COD concentration define the k_S value. It rises as substrate removal efficiency improves. In this study, the k_S values for COD were 0.1062 per day. In a research by [58], the k_S, determined was 3.582 per day. The coefficient of correlation (R^2) of the plot for COD, NH_4^+-N, and TP removal was 0.9985, 0.9982, and 0.9980 respectively. Similarly, A and B were found to have exceptional (R^2) 0.995 correlation coefficients with values of 0.047 and 1.007, respectively. Earlier studies have shown that the COD second-order model constants for treating industrial wastewater with ammonia were $k_s = 10^{-5}$. The model's characteristics and the values of the coefficients indicate a strong correlation coefficient ($R^2 = 0.97$). The results ascribed to this model fit the ammonia data well [44].
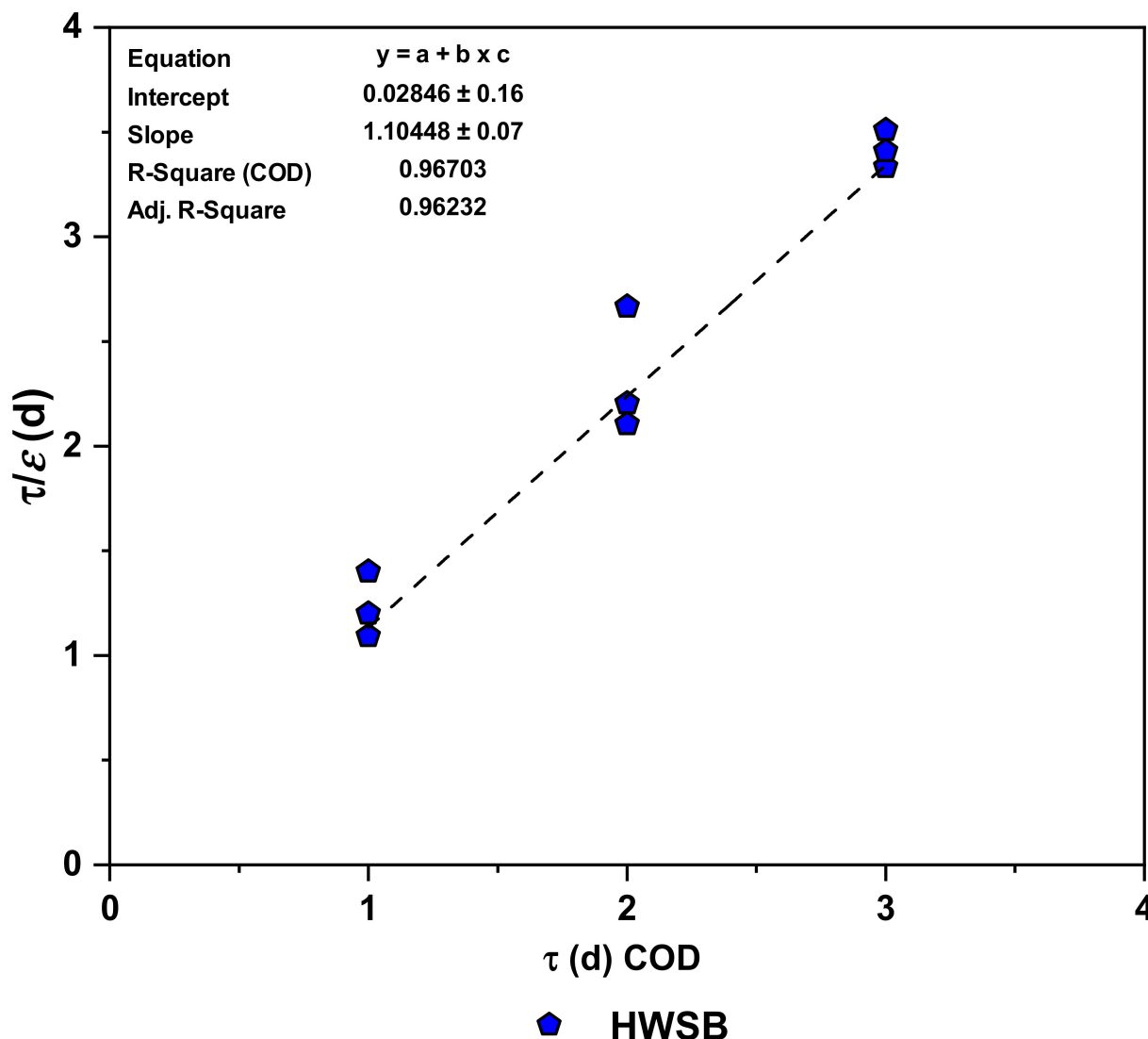
Figure 11. Second-order kinetic plot of COD for CFBS.

4. Conclusions

Agro-industries effluents with high COD and color concentrations discharged into the ecosystem affect aquatic life, human health, and visual intrusion. Thus, the AIE requires treatment prior to discharge. Therefore, the effectiveness of CFBS in the treatment of AIE using HWSB was investigated. The prepared HWSB performance was assessed in terms of COD and color removal efficiency and rate constant. During the evaluation, the influence of AIE concentration and HRT on CFBS performance was investigated. The use of CFBS with HRT of 1–3 days and 10–50% AIE concentrations was adopted in experiments based on a statistical design. For experimental design, optimization, and analysis, RSM was used. The performance of CFBS was analyzed in terms of COD and color removal. Findings indicated 76.52% and 66.97% reduction in COD and color, respectively. Maximum contaminants elimination was attained at 30% AIE and 2-day HRT. Thus, the results obtained from CFBS containing HWSB demonstrated that the system's better performance in the elimination of COD and color resulted from the combined biological and biosorption phenomena. Three distinct kinetic models were used in the study to assess the different processes, and the modified Stover model exhibited the best match with a respectable R^2 value of 0.9741 for COD. It was discovered that the kinetic rate of biosorption was influenced by internal surface diffusion on the adsorbent's solid surface together with the film diffusion and

biosorption rate. Generally, biochar has an advantage in removing COD and color from AIE due to its high surface area, huge spectrum of pore size dispersion, and hydrophobic surface. Therefore, combined with optimal bioreactor design, this method may have some beneficial industrial-scale applications as a tertiary treatment in the current system of AIE treatment for COD and color removal.

References

1. Hernández, D.; Riaño, B.; Coca, M.; García-González, M. Treatment of agro-industrial wastewater using microalgae–bacteria consortium combined with anaerobic digestion of the produced biomass. *Bioresour. Technol.* **2013**, *135*, 598–603. [CrossRef] [PubMed]
2. Amor, C.; Marchão, L.; Lucas, M.S.; Peres, J.A. Application of advanced oxidation processes for the treatment of recalcitrant agro-industrial wastewater: A review. *Water* **2019**, *11*, 205. [CrossRef]
3. Sekeri, S.H.; Ibrahim, M.N.M.; Umar, K.; Yaqoob, A.A.; Azmi, M.N.; Hussin, M.H.; Othman, M.B.H.; Malik, M.F.I.A. Preparation and characterization of nanosized lignin from oil palm (Elaeis guineensis) biomass as a novel emulsifying agent. *Int. J. Biol. Macromol.* **2020**, *164*, 3114–3124. [CrossRef] [PubMed]
4. Libutti, A.; Gatta, G.; Gagliardi, A.; Vergine, P.; Pollice, A.; Beneduce, L.; Disciglio, G.; Tarantino, E. Agro-industrial wastewater reuse for irrigation of a vegetable crop succession under Mediterranean conditions. *Agric. Water Manag.* **2018**, *196*, 1–14. [CrossRef]
5. Teh, C.Y.; Wu, T.Y.; Juan, J.C. Optimization of agro-industrial wastewater treatment using unmodified rice starch as a natural coagulant. *Ind. Crops Prod.* **2014**, *56*, 17–26. [CrossRef]
6. Abubakar, S.; Lawal, I.; Hassan, I.; Jagaba, A. Quality water analysis of public and private boreholes (a case study of Azare Town, Bauchi, Nigeria). *Am. J. Eng. Res.* **2016**, *5*, 204–208.
7. Chen, W.; Oldfield, T.L.; Patsios, S.I.; Holden, N.M. Hybrid life cycle assessment of agro-industrial wastewater valorisation. *Water Res.* **2020**, *170*, 115275. [CrossRef]
8. Yaqoob, A.A.; Noor, N.H.M.; Umar, K.; Adnan, R.; Ibrahim, M.N.M.; Rashid, M. Graphene oxide–ZnO nanocomposite: An efficient visible light photocatalyst for degradation of rhodamine B. *Appl. Nanosci.* **2021**, *11*, 1291–1302. [CrossRef]
9. Bajpai, P. Biological Treatment of Pulp and Paper Mill Effluents. In *Biotechnology for Pulp and Paper Processing*; Springer: Singapore, 2018; pp. 313–369.
10. Jagaba, A.H.; Kutty, S.R.M.; Noor, A.; Affam, A.C.; Ghfar, A.A.; Usman, A.K.; Lawal, I.M.; Birniwa, A.H.; Kankia, M.U.; Afolabi, H.K.; et al. Parametric optimization and kinetic modelling for organic matter removal from agro-waste derived paper packaging biorefinery wastewater. *Biomass Convers. Bioref.* **2022**, 1–18. [CrossRef]
11. Yaqoob, A.A.; Parveen, T.; Umar, K.; Mohamad Ibrahim, M.N. Role of nanomaterials in the treatment of wastewater: A review. *Water* **2020**, *12*, 495. [CrossRef]

12. Brink, A.; Sheridan, C.; Harding, K. A kinetic study of a mesophilic aerobic moving bed biofilm reactor (MBBR) treating paper and pulp mill effluents: The impact of phenols on biodegradation rates. *J. Water Process Eng.* **2017**, *19*, 35–41. [CrossRef]

13. Jagaba, A.H.; Kutty, S.R.M.; Noor, A.; Isah, A.S.; Lawal, I.M.; Birniwa, A.H.; Usman, A.K.; Abubakar, S. Kinetics of Pulp and Paper Wastewater Treatment by High Sludge Retention Time Activated Sludge Process. *J. Hunan Univ. Nat. Sci.* **2022**, *49*, 242–251. [CrossRef]

14. Birniwa, A.H.; Abubakar, A.S.; Huq, A.O.; Mahmud, H.N.M.E. Polypyrrole-polyethyleneimine (PPy-PEI) nanocomposite: An effective adsorbent for nickel ion adsorption from aqueous solution. *J. Macromol. Sci. Part A* **2021**, *58*, 206–217. [CrossRef]

15. Nasara, M.A.; Zubairu, I.; Jagaba, A.H.; Azare, A.A.; Yerima, Y.M.; Yerima, B. Assessment of Non-Revenue Water Management Practices in Nigeria (A Case Study of Bauchi State Water and Sewerage Cooperation). *Am. J. Eng. Res.* **2021**, *10*, 390–401.

16. Birniwa, A.H.; Abubakar, A.S.; Mahmud, H.N.M.E.; Kutty, S.R.M.; Jagaba, A.H.; Abdullahi, S.S.A.; Zango, Z.U. Application of Agricultural Wastes for Cationic Dyes Removal from Wastewater. In *Textile Wastewater Treatment*; Springer: Singapore, 2022; pp. 239–274.

17. Sayed, K.; Baloo, L.; Yekeen, S.T.; Kankia, M.U.; Jagaba, A.H. Determination of Total Petroleum Hydrocarbons Concentration in Coastal Seawater of Teluk Batik Beach, Perak, Malaysia. In *Key Engineering Materials*; Trans Tech Publications: Zurich, Switzerland, 2021; pp. 119–128.

18. Nguyen, M.D.; Thomas, M.; Surapaneni, A.; Moon, E.M.; Milne, N.A. Beneficial reuse of water treatment sludge in the context of circular economy. *Environ. Technol. Innov.* **2022**, *28*, 102651. [CrossRef]

19. Baloo, L.; Isa, M.H.; Sapari, N.B.; Jagaba, A.H.; Wei, L.J.; Yavari, S.; Razali, R.; Vasu, R. Adsorptive removal of methylene blue and acid orange 10 dyes from aqueous solutions using oil palm wastes-derived activated carbons. *Alex. Eng. J.* **2021**, *60*, 5611–5629. [CrossRef]

20. Al-Mahbashi, N.M.Y.; Kutty, S.R.M.; Bilad, M.R.; Huda, N.; Kobun, R.; Noor, A.; Jagaba, A.H.; Al-Nini, A.; Ghaleb, A.A.S.; Al-dhawi, B.N.S. Bench-Scale Fixed-Bed Column Study for the Removal of Dye-Contaminated Effluent Using Sewage-Sludge-Based Biochar. *Sustainability* **2022**, *14*, 6484. [CrossRef]

21. Jagaba, A.H.; Kutty, S.R.M.; Baloo, L.; Noor, A.; Abubakar, S.; Lawal, I.M.; Umaru, I.; Usman, A.K.; Kumar, V.; Birniwa, A.H. Effect of Hydraulic Retention Time on the Treatment of Pulp and Paper Industry Wastewater by Extended Aeration Activated Sludge System. In Proceedings of the 2021 Third International Sustainability and Resilience Conference: Climate Change, Online, 15–16 November 2021; pp. 221–224.

22. Nuanhchamnong, C.; Kositkanawuth, K.; Wantaneeyakul, N. Granular waterworks sludge-biochar composites: Characterization and dye removal application. *Results Eng.* **2022**, *14*, 100451. [CrossRef]

23. Pérez, S.; Giraldo, S.; Forgionny, A.; Flórez, E.; Acelas, N. Eco-Friendly Reuse of Agricultural Wastes to Produce Biocomposites with High Potential in Water Treatment and Fertilizers. *Biomass Convers. Bioref.* **2022**, 1–11. Available online: https://investigaciones-pure.udem.edu.co/en/publications/eco-friendly-reuse-of-agricultural-wastes-to-produce-biocomposite (accessed on 1 September 2022). [CrossRef]

24. Jagaba, A.H.; Kutty, S.R.M.; Hayder, G.; Baloo, L.; Noor, A.; Yaro, N.S.A.; Saeed, A.A.H.; Lawal, I.M.; Birniwa, A.H.; Usman, A.K. A systematic literature review on waste-to-resource potential of palm oil clinker for sustainable engineering and environmental applications. *Materials* **2021**, *14*, 4456. [CrossRef]

25. Noor, A.; Kutty, S.R.M.; Jagaba, A.H.; Yusuf, M.; Akram, M.W.; Adil, M.R.; Ahmad, N.; Jamal, M. Kinetic Modelling of Nutrient Removal of Petroleum Industry Wastewater Remediation. In Proceedings of the 2021 Third International Sustainability and Resilience Conference: Climate Change, Online, 15–16 November 2021; pp. 216–220.

26. Devi, P.; Saroha, A.K. Effect of temperature on biochar properties during paper mill sludge pyrolysis. *Int. J. ChemTech Res.* **2013**, *5*, 682–687.

27. Birniwa, A.; Abdullahi, S. Study on physico-mechanical behaviour of acacia nilotica (gum tree) and glass fiber blend reinforced epoxy resin composite. *ChemSearch J.* **2019**, *10*, 46–53.

28. Witek-Krowiak, A.; Chojnacka, K.; Podstawczyk, D.; Dawiec, A.; Pokomeda, K. Application of response surface methodology and artificial neural network methods in modelling and optimization of biosorption process. *Bioresour. Technol.* **2014**, *160*, 150–160. [CrossRef]

29. Hong, C.; Hao, H.; Haiyun, W. Process optimization for PHA production by activated sludge using response surface methodology. *Biomass Bioenergy* **2009**, *33*, 721–727. [CrossRef]

30. Luo, Y.; Han, Y.; Xue, M.; Xie, Y.; Yin, Z.; Xie, C.; Li, X.; Zheng, Y.; Huang, J.; Zhang, Y. Ball-milled bismuth oxybromide/biochar composites with enhanced removal of reactive red owing to the synergy between adsorption and photodegradation. *J. Environ. Manag.* **2022**, *308*, 114652. [CrossRef]

31. Jagaba, A.; Kutty, S.; Fauzi, M.; Razali, M.; Hafiz, M.; Noor, A. Organic and Nutrient Removal from Pulp and Paper Industry Wastewater by Extended Aeration Activated Sludge System. *IOP Conf. Ser. Earth Environ. Sci.* **2021**, *781*, 012021. [CrossRef]

32. Sharma, P.; Iqbal, H.M.; Chandra, R. Evaluation of pollution parameters and toxic elements in wastewater of pulp and paper industries in India: A case study. *Case Stud. Chem. Environ. Eng.* **2022**, *5*, 100163. [CrossRef]

33. Tian, W.; Gao, Q.; Qian, W. Interlinked porous carbon nanoflakes derived from hydrolyzate residue during cellulosic bioethanol production for ultrahigh-rate supercapacitors in nonaqueous electrolytes. *ACS Sustain. Chem. Eng.* **2017**, *5*, 1297–1305. [CrossRef]

34. Kang, C.; Zhao, Y.; Tang, C.; Addo-Bankas, O. Use of aluminum-based water treatment sludge as coagulant for animal farm wastewater treatment. *J. Water Process Eng.* **2022**, *46*, 102645. [CrossRef]

35. Kankia, M.U.; Baloo, L.; Danlami, N.; Mohammed, B.S.; Haruna, S.; Abubakar, M.; Jagaba, A.H.; Sayed, K.; Abdulkadir, I.; Salihi, I.U. Performance of Fly Ash-Based Inorganic Polymer Mortar with Petroleum Sludge Ash. *Polymers* **2021**, *13*, 4143. [CrossRef]

36. Gupta, V.; Bhardwaj, N.; Rawal, R. Removal of color and lignin from paper mill wastewater using activated carbon from plastic mix waste. *Int. J. Environ. Sci. Technol.* **2022**, *19*, 2641–2658. [CrossRef]

37. Ghaleb, A.; Kutty, S.; Ho, Y.; Jagaba, A.; Noor, A.; Al-Sabaeei, A.; Kumar, V.; Saeed, A. Anaerobic co-digestion for oily-biological sludge with sugarcane bagasse for biogas production under mesophilic condition. *IOP Conf. Ser. Mater. Sci. Eng.* **2020**, *991*, 012084. [CrossRef]

38. Zhang, Y.; Qin, J.; Yi, Y. Biochar and hydrochar derived from freshwater sludge: Characterization and possible applications. *Sci. Total Environ.* **2021**, *763*, 144550. [CrossRef] [PubMed]

39. Kankia, M.U.; Baloo, L.; Danlami, N.; Samahani, W.N.; Mohammed, B.S.; Haruna, S.; Jagaba, A.H.; Abubakar, M.; Ishak, E.A.; Sayed, K. Optimization of Cement-Based Mortar Containing Oily Sludge Ash by Response Surface Methodology. *Materials* **2021**, *14*, 6308. [CrossRef]

40. Sun, C.; Du, Q.; Zhang, X.; Wang, Z.; Zheng, J.; Wu, Q.; Li, Z.; Long, T.; Guo, W.; Ngo, H.H. Role of spent coffee ground biochar in an anaerobic membrane bioreactor for treating synthetic swine wastewater. *J. Water Process Eng.* **2022**, *49*, 102981. [CrossRef]

41. Sayed, K.; Baloo, L.; Kutty, S.R.B.; Al Madhoun, W.; Kankia, M.U.; Jagaba, A.H.; Singa, P.K. Optimization of palm oil mill effluent final discharge as biostimulant for biodegradation of tapis light crude petroleum oil in seawater. *J. Sea Res.* **2022**, *188*, 102268. [CrossRef]

42. Singh, G.; Singh, N.; Shukla, S. Remediation of COD and color from textile wastewater using dual stage electrocoagulation process. *SN Appl. Sci.* **2019**, *1*, 1000. [CrossRef]

43. Puri, S.; Verma, A. Color removal from secondary treated pulp & paper industry effluent using waste driven Fe–TiO2 composite. *Chemosphere* **2022**, *303*, 135143.

44. Abedinzadeh, N.; Shariat, M.; Monavari, S.M.; Pendashteh, A. Evaluation of color and COD removal by Fenton from biologically (SBR) pre-treated pulp and paper wastewater. *Process Saf. Environ. Prot.* **2018**, *116*, 82–91. [CrossRef]

45. Kumar, R.; Singh, A.; Maurya, A.; Yadav, P.; Yadav, A.; Chowdhary, P.; Raj, A. Effective bioremediation of pulp and paper mill wastewater using Bacillus cereus as a possible kraft lignin-degrading bacterium. *Bioresour. Technol.* **2022**, *352*, 127076. [CrossRef]

46. Devi, P.; Saroha, A.K. Risk analysis of pyrolyzed biochar made from paper mill effluent treatment plant sludge for bioavailability and eco-toxicity of heavy metals. *Bioresour. Technol.* **2014**, *162*, 308–315. [CrossRef] [PubMed]

47. Jagaba, A.H.; Kutty, S.R.M.; Salih, G.H.A.; Noor, A.; HAFIZ, M.; Yaro, N.S.A.; Saeed, A.A.H.; Lawal, I.M.; Birniwa, A.H.; Kilaco, A.U. *Palm Oil Clinker as a Waste By-Product: Utilization and Circular Economy Potential*; IntechOpen: London, UK, 2021; Volume 1.

48. Sathian, S.; Rajasimman, M.; Radha, G.; Shanmugapriya, V.; Karthikeyan, C. Performance of SBR for the treatment of textile dye wastewater: Optimization and kinetic studies. *Alex. Eng. J.* **2014**, *53*, 417–426. [CrossRef]

49. Jagaba, A.H.; Kutty, S.R.M.; Isa, M.H.; Affam, A.C.; Aminu, N.; Abubakar, S.; Noor, A.; Lawal, I.M.; Umaru, I.; Hassan, I. Effect of Environmental and Operational Parameters on Sequential Batch Reactor Systems in Dye Degradation. In *Dye Biodegradation, Mechanisms and Techniques*; Springer: Singapore, 2022; pp. 193–225.

50. Saeed, A.A.H.; Harun, N.Y.; Sufian, S.; Bilad, M.R.; Zakaria, Z.Y.; Jagaba, A.H.; Ghaleb, A.A.S.; Mohammed, H.G. Pristine and magnetic kenaf fiber biochar for Cd^{2+} adsorption from aqueous solution. *Int. J. Environ. Res. Public Health* **2021**, *18*, 7949. [CrossRef] [PubMed]

51. Birniwa, A.H.; Abdullahi, S.S.A.; Yakasai, M.Y.; Ismaila, A. Studies on physico-mechanical behaviour of kenaf/glass fiber reinforced epoxy hybrid composites. *Bull. Chem. Soc. Ethiop.* **2021**, *35*, 171–184. [CrossRef]

52. Ghaleb, A.A.S.; Kutty, S.R.M.; Salih, G.H.A.; Jagaba, A.H.; Noor, A.; Kumar, V.; Almahbashi, N.M.Y.; Saeed, A.A.H.; Saleh Al-dhawi, B.N. Sugarcane bagasse as a co-substrate with oil-refinery biological sludge for biogas production using batch mesophilic anaerobic co-digestion technology: Effect of carbon/nitrogen ratio. *Water* **2021**, *13*, 590. [CrossRef]

53. Jagaba, A.H.; Kutty, S.R.M.; Lawal, I.M.; Aminu, N.; Noor, A.; Al-dhawi, B.N.S.; Usman, A.K.; Batari, A.; Abubakar, S.; Birniwa, A.H. Diverse sustainable materials for the treatment of petroleum sludge and remediation of contaminated sites: A review. *Clean. Waste Syst.* **2022**, *2*, 100010. [CrossRef]

54. Lawal, I.M.; Bertram, D.; White, C.J.; Jagaba, A.H.; Hassan, I.; Shuaibu, A. Multi-criteria performance evaluation of gridded precipitation and temperature products in data-sparse regions. *Atmosphere* **2021**, *12*, 1597. [CrossRef]

55. Jagaba, A.H.; Kutty, S.R.M.; Noor, A.; Birniwa, A.H.; Affam, A.C.; Lawal, I.M.; Kankia, M.U.; Kilaco, A.U. A systematic literature review of biocarriers: Central elements for biofilm formation, organic and nutrients removal in sequencing batch biofilm reactor. *J. Water Process Eng.* **2021**, *42*, 102178. [CrossRef]

56. Birniwa, A.H.; Mahmud, H.N.M.E.; Abdullahi, S.S.A.; Habibu, S.; Jagaba, A.H.; Ibrahim, M.N.M.; Ahmad, A.; Alshammari, M.B.; Parveen, T.; Umar, K. Adsorption Behavior of Methylene Blue Cationic Dye in Aqueous Solution Using Polypyrrole-Polyethylenimine Nano-Adsorbent. *Polymers* **2022**, *14*, 3362. [CrossRef]

57. Al-mahbashi, N.; Kutty, S.; Jagaba, A.; Al-Nini, A.; Ali, M.; Saeed, A.; Ghaleb, A.; Rathnayake, U. Column Study for Adsorption of Copper and Cadmium Using Activated Carbon Derived from Sewage Sludge. *Adv. Civ. Eng.* **2022**, *2022*, 3590462. [CrossRef]

58. Ghaleb, A.A.S.; Kutty, S.R.M.; Ho, Y.-C.; Jagaba, A.H.; Noor, A.; Al-Sabaeei, A.M.; Almahbashi, N.M.Y. Response surface methodology to optimize methane production from mesophilic anaerobic co-digestion of oily-biological sludge and sugarcane bagasse. *Sustainability* **2020**, *12*, 2116. [CrossRef]